A constitutive model for strain rates from 10^{-4} to 10^{6} s^{-1}

D. J. Steinberg and C. M. Lund
Lawrence Livermore National Laboratory, P.O. Box 808, Livermore, California 94550

(Received 18 April 1988; accepted for publication 12 October 1988)

We have developed an addition to the Steinberg–Guinan high strain-rate constitutive model that extends its validity to strain rates as low as 10^{-4} s^{-1}. With this new model, we have successfully reproduced a number of rate-dependent, shock-induced phenomena in tantalum, such as precursor on reshock, precursor decay, and shock smearing. We have also successfully calculated a plate-impact experiment at a loading stress of 230 GPa as well as extensive data for yield strength versus strain rate at room temperature and yield strength versus temperature at a strain rate of 10^{-4} s^{-1}.

I. INTRODUCTION

In a series of papers,[1–3] Steinberg and co-workers described a constitutive model for use with hydrodynamic computer codes. The model, valid for high deformation rates, accounts for pressure and temperature dependence of the yield strength and shear modulus, work hardening, pressure-dependent melting, Bauschinger and strain-rate effects, and spall.

Steinberg[3] has also discussed the model's major deficiencies, such as its failure to predict the elastic precursor seen on reshock in such materials as Be,[4] W,[5] and Al.[6] A second deficiency is in the rate dependence, where the stress deviator is a function of thermal energy (temperature) and strain rate. This part of the model requires three parameters, two of which must be determined through normalization against at least one shock-wave experiment. In addition, one of these parameters does not have any obvious physical meaning. A third drawback is that the Bauschinger model cannot be generalized to 2D and 3D hydrodynamic codes. Finally, the model neither predicts precursor decay nor addresses any low strain-rate phenomena.

Using the work of Hoge and Mukherjee,[7] we have added a new strain-rate modification to our model that extends its validity to strain rates as low as 10^{-4} s^{-1}. We have successfully reproduced data for tantalum showing precursor decay as well as shock smearing, i.e., the slow increase in stress between the precursor and the main shock. While there are no reshock data for Ta, the model predicts an elastic wave preceding the second shock. The model also successfully reproduces a plate-impact experiment at a loading stress of 230 GPa as well as the extensive data of Hoge and Mukherjee on yield strength Y versus temperature T at a constant plastic strain-rate $\dot{\epsilon}_p$ and Y vs $\dot{\epsilon}_p$ at constant T.

II. YIELD-STRENGTH MODEL AND COMPARISON WITH LOW STRAIN-RATE DATA

We write the yield strength as

$$Y = [\,Y_T(\dot{\epsilon}_p,T) + Y_A f(\epsilon_p)\,][G(P,T)/G_0], \qquad (1)$$

where $Y_T(\dot{\epsilon}_p,T)$ is the thermally activated part of the yield strength and is a function of $\dot{\epsilon}_p$ and T. The second, or athermal, term is similar in form to the Steinberg–Guinan model,[1] with $f(\epsilon_p)$, the work-hardening term, a function of the equivalent plastic strain ϵ_p and $G(P,T)/G_0$, the pressure P and temperature-dependent shear modulus divided by G_0, the modulus at STP conditions. For close-packed structures, where the first term in Eq. (1) is small, this relationship reduces to the Steinberg–Guinan model with Y_A equal to the yield strength at the Hugoniot elastic limit Y_0. However, for BCC and other structures, the thermally activated component can be large.

Following Hoge and Mukherjee, we write $\dot{\epsilon}_p(Y_T,T)$ as

$$\dot{\epsilon}_p = \left\{\frac{1}{C_1}\exp\left[\frac{2U_K}{kT}\left(1-\frac{Y_T}{Y_P}\right)^2\right]+\frac{C_2}{Y_T}\right\}^{-1}. \qquad (2)$$

Here Y_P is the Peierls stress, $2U_K$ is the energy to form a pair of kinks in a dislocation segment of length L, and k is the Boltzmann constant. The constant C_2 is the drag coefficient D divided by the dislocation density ρ times the square of the Burgers' vector b. The constant C_1 is

$$C_1 = \rho L a b^2 \nu/2\ w^2, \qquad (3)$$

where a is the distance between Peierls valleys, w is the width of a kink loop, and ν is the Debye frequency. Finally, we limit Y_T to be $\leqslant Y_P$.

Following Wilkins,[8] the stress deviators s_{ij} are updated from a finite-difference representation of

$$\dot{s}_{ij} = 2G\dot{\theta}_{ij} - (3G/Y)\dot{\epsilon}_p s_{ij}, \qquad (4)$$

where $\dot{\theta}_{ij}$ is the strain-rate deviator. This equation is consistent with

$$\dot{\epsilon}_p = \sqrt{\tfrac{2}{3}\dot{\epsilon}^p_{ij}\dot{\epsilon}^p_{ij}},$$
$$\dot{\epsilon}^p_{ij} = \dot{\theta}_{ij} - \dot{s}_{ij}/2G.$$

If $\dot{s}_{ij}/2G$ is negligible compared to $\dot{\theta}_{ij}$, $\dot{\epsilon}_p$ can be interpreted as a physical strain rate defined in terms of velocity gradients. Hoge and Mukherjee did not explicitly state whether $\dot{\epsilon}_p$ in Eq. (2) was defined as above, or whether they defined it solely in terms of $\dot{\theta}_{ij}$ during plastic strain. We assume that either interpretation is equivalent to within the accuracy of the model.

Because Y is a function of $\dot{\epsilon}_p$, and $\dot{\epsilon}_p$ is a relatively noisy quantity in a numerical calculation, we found that care was necessary in the choice of the finite-difference form of Eq. (4) in order that code calculations be done efficiently. The strain-rate deviators $\dot{\theta}_{ij}$ are known from the acceleration calculations, and $\dot{\epsilon}_p$ is determined by the yield condition $s_{ij}s_{ij} \leqslant 2/3Y^2$, and $\dot{\epsilon}_p \geqslant 0$. Denoting variables to be updated over interval δt with primes, we difference Eq. (4) as

 0021-8979/89/041528-06$02.40

$$s'_{ij} - s_{ij} = \{2G\dot{\theta}_{ij} - [3G/Y(\dot{\epsilon}'_p)]\dot{\epsilon}'_p s'_{ij}\}\delta t, \quad (5)$$

$$\epsilon'_p - \epsilon_p = \dot{\epsilon}'_p \delta t, \quad (6)$$

where $\dot{\epsilon}'_p$ is evaluated from the yield condition written in terms of the new values. This is the same as Wilkins' expression, except that Y is now a function of $\dot{\epsilon}_p$, evaluated at the end of the time interval in Eq. (5). We found it is important for numerical stability, at time steps large enough to run efficiently, that the newest value of $\dot{\epsilon}_p$ be used in Y.

As is customary, we introduce an auxiliary variable $\hat{s}_{ij}$ defined by

$$\hat{s}_{ij} - s_{ij} = 2G\dot{\theta}_{ij}\delta t. \quad (7)$$

One notes that $\hat{s}_{ij}$ does not depend on $\dot{\epsilon}'_p$, and hence can be solved for before $\dot{\epsilon}'_p$ is known. Furthermore, s'_{ij} is proportional to $\hat{s}_{ij}$,

$$s'_{ij} = \hat{s}_{ij}/\{1 + [3G/Y(\dot{\epsilon}'_p)]\dot{\epsilon}'_p \delta t\}.$$

Once $\dot{\epsilon}'_p$ is known, one gets s'_{ij} by scaling.

The scale factor is determined by the yield condition, but this implicitly involves $\dot{\epsilon}'_p$. A single relation between $Y(\dot{\epsilon}'_p)$ and $\dot{\epsilon}'_p$ is found by subtracting the equations for $\hat{s}_{ij}$ and s'_{ij}, multiplying by s'_{ij}, and summing. This leads to

$$\dot{\epsilon}'_p = \left[\sqrt{\tfrac{3}{2}}\hat{s} - Y(\dot{\epsilon}'_p)\right]/3G\,\delta t, \quad (8)$$

if $\sqrt{\frac{3}{2}}\hat{s} > Y(0)$, where $\hat{s} = \sqrt{\hat{s}_{ij}\hat{s}_{ij}}$.

This equation can be solved efficiently by noting that $Y(\dot{\epsilon}_p)$ monotonically increases with $\dot{\epsilon}_p$. Therefore, a solution exists such that

$$0 < \dot{\epsilon}'_p < \left[\sqrt{\tfrac{3}{2}}\hat{s} - Y(0)\right]/3G\,\delta t.$$

Equation (2) gives $\dot{\epsilon}_p = \dot{\epsilon}_p(Y_T)$, and Eq. (1) gives $Y = Y(Y_T)$, with all other variables on the right-hand side of Eqs. (1) and (2) determined. Therefore, Eq. (8) can be explicitly written as a single equation determining Y'_T, the value of Y_T at the end of the cycle. A carefully coded binary-chop/Newton's iteration algorithm was able to solve this equation for Y'_T on a Cray XMP with calculations that averaged roughly 5 μs per zone cycle using approximately four iterations to find the solution to within one part in 10^6.

Equation (2) is not original with Hoge and Mukherjee, but follows from the work of Dorn and co-workers.[9–11] Hoge and Mukherjee give values for the various dislocation parameters which are $a \approx b = 2.86\times10^{-10}$ m, $L = 10^4 b$, $w = 24b$, $U_K = 0.31$ eV, $D = 10^{-10}$ MPa s, $\rho = 10^{11}$ m^{-2}, $\nu = 10^{13}$ s^{-1}, and $Y_P = 1$ GPa. This implies that $C_1 = 0.71\times10^6$ s^{-1} and $C_2 = 0.012$ MPa s. (These data are not referenced, but earlier unpublished versions of Ref. 7 do give some of the sources: b and L from Ref. 9, w and U_K from Ref. 10, and D from Ref. 11.)

Hoge and Mukherjee have taken extensive data on Ta, including Y_T vs $\dot{\epsilon}_p$ from 10^{-4} to 2×10^4 s^{-1} at $T = 300$ K, and Y_T vs T from 23 to 800 K at $\dot{\epsilon}_p = 10^{-4}$ s^{-1}. Figures 1 and 2 compare these data with calculations using Eq. (2). The value for Y_P has been changed to 0.88 GPa, still within the uncertainty, because it gave a better fit to the Y_T vs $\dot{\epsilon}_p$ data. In addition, it is principally the single point at 23 K (Fig. 2) that implies $Y_P = 1$ GPa. Hoge and Mukherjee never refer to this point in the text, even describing their data as starting at 78 K. It is possible to keep $Y_P = 1$ GPa and still get good agreement with the data if C_1 is changed to 0.2×10^6 s^{-1}. However, using the lower value of Y_P also produces better agreement with the shock-wave data.

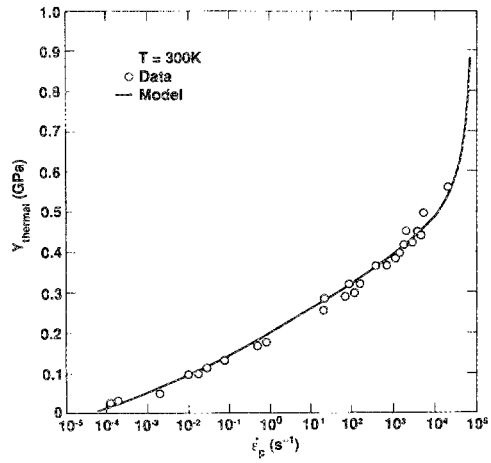

FIG. 1. Comparison of Ta experimental data and Eq. (2) for Y_T vs $\dot{\epsilon}_p$ at $T = 300$ K.

Considering that the values for many of the dislocation parameters are not well known, it is surprising that Eq. (2) fits the data as well as it does. This is why shock-wave data are so important, as they can provide an independent test of the model.

III. COMPARISON OF THE MODEL WITH SHOCK-WAVE DATA

Isbell, Christman, and Babcock,[12] did an extensive study of the dynamic properties of Ta. Included is a quartz-gauge study of elastic precursor decay. In the Steinberg–Guinan model,[1] Y_0 was determined by normalizing to the knee of the wave profile measured 15.25 mm from the impact surface. This gave $Y_0 = 0.77$ GPa. The parameter Y_A in Eq. (1) can be determined in a like manner and was found to be 0.375 GPa, about one-half of Y_0. To do the calculation, we used a Mie–Gruneisen equation of state and the Hugoniot summary of McQueen *et al.*[13] The other required parameters can be found in Ref. 1.

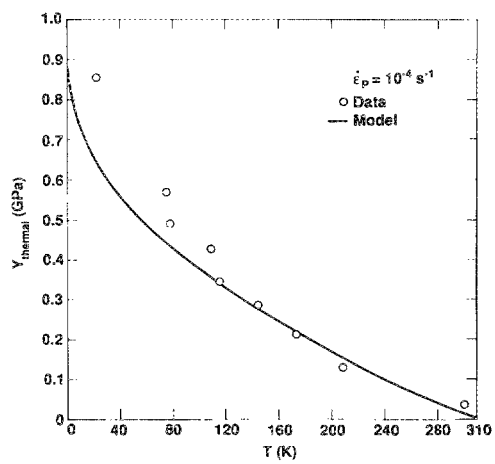

FIG. 2. Comparison of Ta experimental data and Eq. (2) for Y_T vs T at $\dot{\epsilon}_p = 10^{-4}$ s^{-1}.

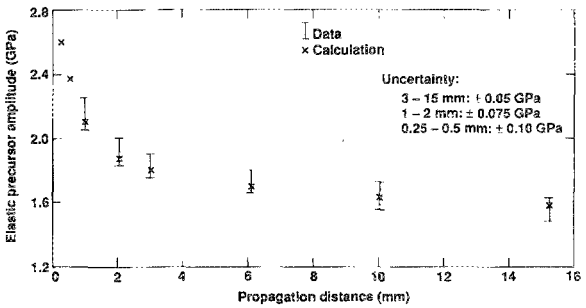

FIG. 3. Comparison of the experimental elastic precursor amplitude and calculation for Ta using the rate-dependent constitutive model.

Figure 3 shows the precursor decay data at 1.01, 2.06, 3.01, 6.11, 10.07, and 15.25 mm as vertical lines which express the uncertainty in determining the knee in the experimental profiles. The calculations, using Eqs. (1) and (2) with $Y_A = 0.375$ GPa, are also shown. To avoid clutter, the calculations are displayed as single values representing our best estimate of the knee. The uncertainties in the calculations are listed separately in Fig. 3. With $Y_A = 0.375$ GPa, the agreement from 1 to 10 mm is excellent.

In the course of a spall study, Banner[14] performed several plate-impact experiments on Ta. The initial conditions for the highest and lowest stress experiments are given in Table I. A third wave profile, at a slightly higher initial stress, was taken from the work of Taylor.[15] We will use these profiles, in particular the shape of the loading wave, to test our model. Finally, to show that the model can successfully handle very strong shocks, we will compare the data of Grady[16] with calculation (maximum stress equals 230 GPa).

Figures 4–6 compare the data for the Banner and Taylor experiments with the calculations using Eqs. (1) and (2) and the constants C_1, C_2, U_K, Y_P, and Y_A determined from the previous data. The experimental profiles have been normalized in velocity at the calculated maximum. However, these changes, averaging $\frac{3}{4}$%, are well within the absolute accuracy of the measurement techniques.

The parameter Y_A depends on the purity and thermomechanical history of the sample material. Hoge and Mukherjee give $Y_A = 0.124$ GPa for their 99.9% fully recrystalized samples. Isbell, Christman, and Babcock state that their samples are 99.5% Ta and that annealing at 1200 °C for 1 h did not make a significant change in the structure or hardness when compared to the as-received material; grain

TABLE I. Initial conditions for the four shock-wave experiments and calculated maximum stress, strain rate, and temperature increase reached midway in the shocked targets. X_F is the thickness of the flyer, V_F its velocity, and X_t the target thickness.

Experiment	X_F (mm)	X_t (mm)	V_F (mm/μs)	σ (GPa)	$\dot{\epsilon}_p$ (s^{-1})	ΔT (K)
Banner 1	3.005	6.003	0.161	5	5.1×10^4	17
Banner 2	3.006	6.009	0.232	7.2	3.2×10^5	27
Taylor	3.05	9.60	0.390	12.1	9.4×10^5	49
Grady	1.013	1.388	3.5	230	3.3×10^7	7500

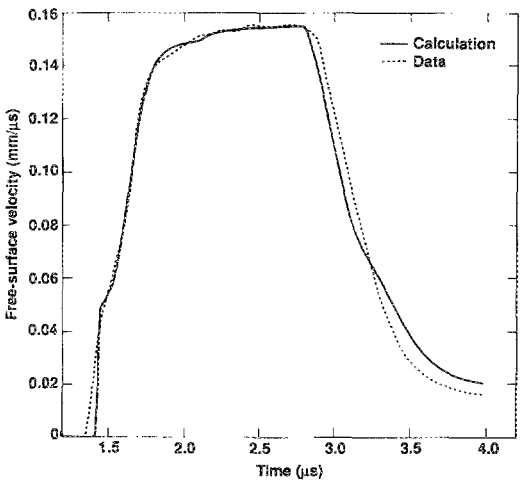

FIG. 4. Comparison of calculation and experiment for a Ta target shocked to a peak stress of 5 GPa. The experimental profile has been reduced by 1% to normalize it to the calculation at the maximum velocity.

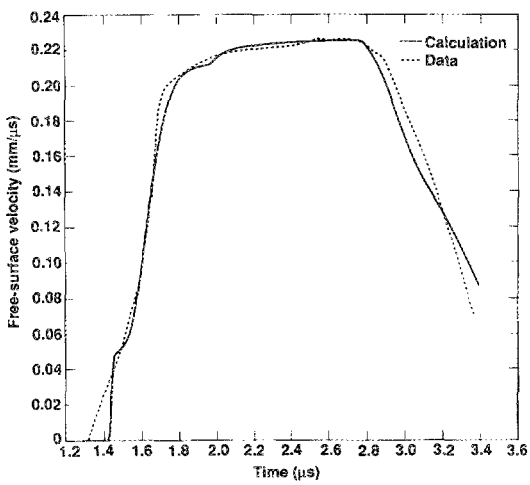

FIG. 5. Comparison of calculation and experiment for a Ta target shocked to a peak stress of 7.2 GPa.

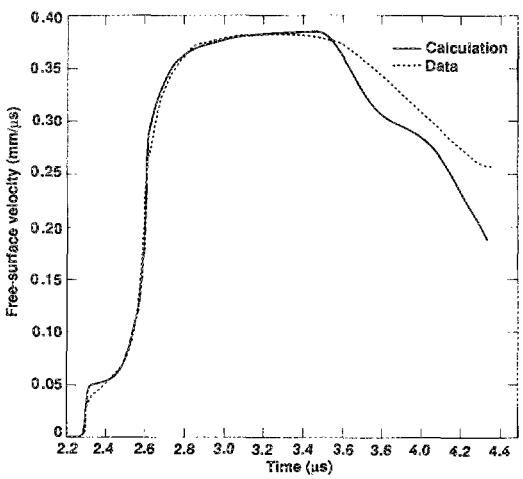

FIG. 6. Comparison of calculation and experiment for a Ta target shocked to a peak stress of 12.1 GPa. The experimental profile has been increased by 1.3% to normalize it to the calculation at the maximum velocity.

size ranged from 45 to 500 μm. Nothing is known about the material in the other shock-wave experiments. Therefore, we have made the assumption that all samples in the shock-wave experiments are similar.

The data of Banner do not show a clear elastic precursor. This could imply either that the material is different from that used in the precursor decay studies or simply that the experiments, which used the free-surface capacitor technique, were unable to satisfactorily resolve the precursor. Consequently, we normalized the calculations in time to the experimental plastic loading wave.

The agreement between experiment and calculation is excellent for the loading portion of the waves but not as good for the release profiles, particularly the Taylor data. However, the data for the two highest stress experiments clearly showed spall reverberations, and the spall may affect the shape of the release profiles. (We have shown the data only up to the pull-back minimum.)

For the experiments of Banner, the release-wave timing also shows slight disagreements. The calculated release wave arrives at the same time as the first break or drop in the data. However, the data also show a second break; it is not clear what this means. New experiments, without spall, would help resolve whether the disagreements stem primarily from experimental or calculational shortcomings.

Figure 7 compares the lower-stress experiment of Banner with calculations done with the rate-independent model.[1] It is clear that the rate dependence smooths both the loading and unloading profiles and that calculations using the new model agree much better with the data.

Figure 8 shows the 230-GPa experiment compared with our calculation. The overall agreement is excellent. However, this experiment is at such a high stress level that it is not a sensitive test of the model. Calculations with the rate-independent model, in combination with the Bauschinger model, produce an equally good fit to the data.[3] This is because at 230 GPa, the deviator is only $\sim 1\%$ of the total stress. For example, at midtarget, the peak stress in the rate-dependent model is only 0.2% higher than with the rate-independent model and only $\sim 2\%$ higher during the elastic release. Even

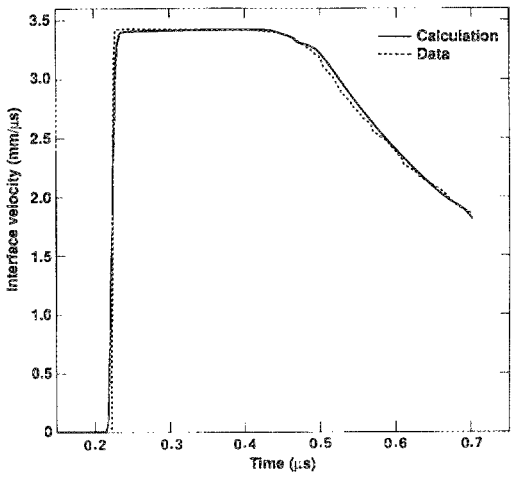

FIG. 8. Comparison of calculation and experiment for a Ta target shocked to a peak stress of 230 GPa. The experimental profile has been reduced by 0.7% to normalize it to the calculation at the maximum velocity.

at the Ta-LiF interface the maximum difference in stress does not exceed 3%. These differences are too small to be clearly distinguished experimentally.

IV. DISCUSSION

A rate-dependent yield strength means that an equilibrium state cannot exist and that flat-topped waves can never be perfectly flat. Figure 9 illustrates this for the two experiments of Banner where calculated Y and Y_T are plotted versus time. At these low stress levels, the effects of P and T on G are small. In addition, Ta does not exhibit significant work hardening. Therefore, we would expect the athermal component of Y to be nearly constant $\approx Y_A$. It is clear from Fig. 9 that the time dependence of Y is determined almost solely from Y_T.

Because of the small amount of work hardening, Ta is not expected to show a large Bauschinger effect. This is borne out in the reverse loading or compression-tension data in Ref. 12. Figure 7 shows a calculation with the rate-independent model plus the Bauschinger effect. We have used

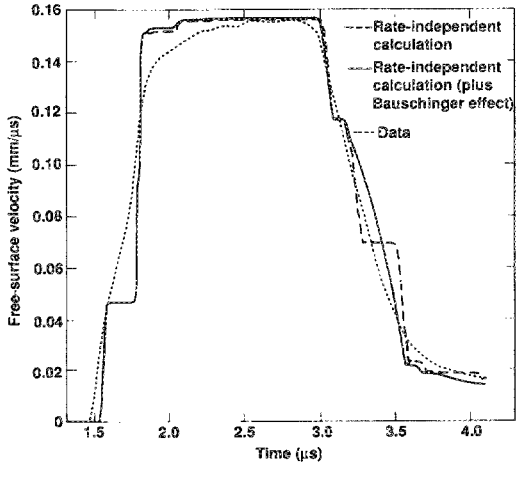

FIG. 7. Comparison of the 5-GPa peak stress experiment with calculations done with the older, rate-independent model.

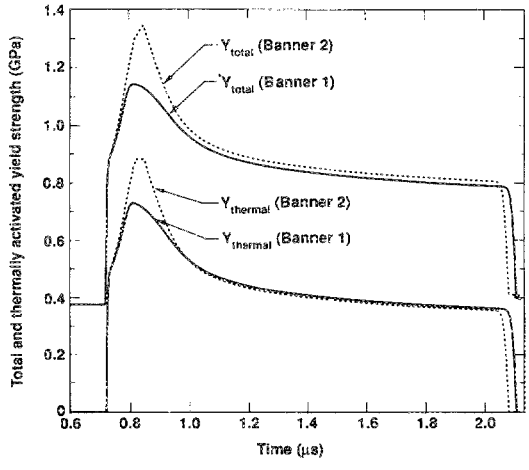

FIG. 9. Y and Y_T vs time for the two experiments of Banner calculated at the midpoint of the target.

the simplest version of our Bauschinger model, where the Bauschinger effect does not commence until the hydrostat is crossed on release.[1] It is clear that the addition of the Bauschinger model improves the fit to the data, but it is still not as smooth or as well shaped as the calculation with the rate-dependent model (see Fig. 4).

By its very nature, the rate-dependent model will not act the same during release as it did during loading, therefore, it contains the basic feature of a Bauschinger effect. Nevertheless, all three of the low-pressure shock-wave experiments still show smoother release profiles than do the calculations. As we have already mentioned, the release data may not be adequate to say whether we need an additional Bauschinger model. If we could dispense with this addition, it would considerably simplify the total constitutive model.

Because Y is a function of $\dot{\epsilon}_p$, the new model predicts that an elastic precursor will be evident before the arrival of a second shock in a double-shock experiment. Figure 10 shows the results of two hypothetical experiments. In the first, a Ta flyer strikes a Ta target, so that both shock loading and unloading occur. In the second experiment, the Ta flyer is backed with iridium, so that the target undergoes a double shock. Both the new rate-dependent model and the rate-independent model, the latter with the Bauschinger effect, were used to calculate these hypothetical cases.

In the second experiment with the rate-independent model, the Ta is first shocked to ~ 11 GPa and then to ~ 13 GPa. Immediately after the first shock, the target is in equilibrium and the stress deviator always at the yield surface. Therefore, there will be no elastic precursor. However, the situation is quite different when the new model is used. Because $\dot{\epsilon}_p$ is very low after the arrival of the first shock, Y_T is small and so is Y. With the arrival of the elastic precursor, Y_T and Y increase and a definite two-wave structure becomes apparent. The calculation still puts the stress deviator on the yield surface, but the surface is now changing.

Table I lists the calculated maximum values of $\dot{\epsilon}_p$ and increases in temperature that are achieved in the four shock-wave experiments. The temperatures were calculated from the thermal energy and a constant specific heat equal to three times the gas constant. For small temperatures, within 50 K of room temperature, this choice of specific heat is quite reasonable.

Grady's experiment is in a different regime of T and $\dot{\epsilon}_p$. The value for ΔT in Table I merely shows that a 230-GPa shock produces very high temperatures; once T gets large enough, Y_T becomes so small that the exact value of T becomes unimportant. Even at this high temperature though, the material has not melted.[3] The calculated value of $\dot{\epsilon}_p$ in this experiment does not represent any true measure of strain rate because the artificial viscosity and zoning in the hydrocode now dominate any real viscosity. There is also evidence that the artificial viscosity has some effect in Taylor's experiment. Consequently, while the hydrocode can simulate Grady's experiment, the new rate-dependent model cannot be justified physically beyond $\dot{\epsilon}_p \approx 10^6\ \mathrm{s}^{-1}$. Finally, in the calculation of Grady's experiment, Y did not exceed 3.7 GPa. This is about $\frac{1}{20}$ of the initial shear modulus, which is a very reasonable maximum.

The maximum values of $\dot{\epsilon}_p$ for the three low-pressure experiments range from 5×10^4 to $10^6\ \mathrm{s}^{-1}$. This is the range between the highest strain-rate Hopkinson-bar data and the beginning of strong shock experiments, or where our understanding is probably the weakest. We have used low strain-rate data to construct a model to predict shock-wave experiments. It should be possible to reverse the procedure and use quality, time-resolved shock-wave data to help improve the models and to refine the parameters for lower strain-rate phenomena.

As an example, Fig. 11 shows three calculations of the 5-GPa experiment using three different values for D. Because C_1, U_K, Y_P, and Y_A could be tested against other data, D (or C_2) appears to be the least well-known parameter. The central curve is the same calculation as shown in Fig. 4 with $D = 10^{-10}$ MPa s. The more steeply rising loading curve uses a quarter of this value, the more gradual curve, twice the value. The parameter C_2 is not known to a factor of 8, but this difference is easily seen in the figure.

V. CONCLUSIONS

We have developed an addition to the Steinberg–Guinan high strain-rate constitutive model[1] that extends its

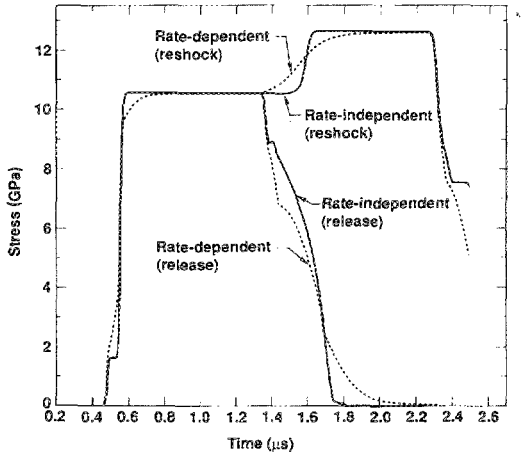

FIG. 10. Comparison of a pair of hypothetical shock/release and shock/reshock experiments calculated with the rate-independent (plus Bauschinger effect) and the rate-dependent models.

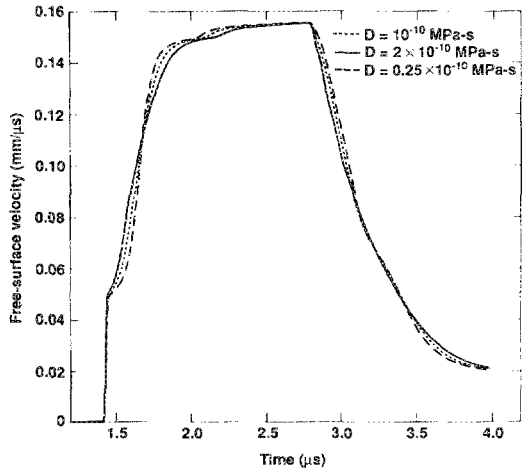

FIG. 11. Comparison of three calculations of the 5-GPa experiment using different values of the dislocation drag coefficient.

validity to strain rates as low as $10^{-4}\ s^{-1}$. This was done by splitting the yield strength into thermal and athermal components, where the former is a function of strain rate and temperature. We have used the work of Hoge and Mukherjee[7] to determine the thermally activated part of the yield strength.

This model is simpler than our previous work on strain-rate dependence[2] and has fewer coefficients which must be determined through normalization to shock-wave experiments. The hydrocode calculations run very stably and efficiently. Models for the thermally activated part of the yield strength other than that of Hoge and Mukherjee could easily be substituted, provided they can be expressed as $\dot{\epsilon}_p = f(Y_T, T)$.

With the new model, we have successfully reproduced a number of rate-dependent, shock-induced phenomena in tantalum, including precursor on reshock, precursor decay, and shock smearing. There are no shock and reshock data for tantalum, but the phenomenon of precursor on reshock has been observed in other metals.

The model also successfully reproduces a plate-impact experiment at a loading stress of 230 GPa as well as extensive data for yield strength versus strain rate from 10^{-4} to 2×10^{4} s^{-1} at room temperature and yield strength versus temperature from 23 to 800 K at a strain rate of $10^{-4}\ s^{-1}$.

Therefore, it appears that this model will reproduce data at strain rates from 10^{-4} to $\sim10^{6}\ s^{-1}$. The model could provide a bridge between the microscopic studies of metallurgy and the macroscopic experiments of shock-wave physics.

ACKNOWLEDGMENTS

We would like to thank Dr. Michael Guinan for his counsel during the course of this investigation. This work was performed under the auspices of the U.S. Department of Energy by the Lawrence Livermore National Laboratory under Contract No. W-7405-Eng-48.

[1] D. J. Steinberg, S. G. Cochran, and M. W. Guinan, J. Appl. Phys. **51**, 1498 (1980).
[2] D. J. Steinberg and R. W. Sharp, J. Appl. Phys. **52**, 5072 (1981).
[3] D. J. Steinberg, Int. J. Impact Eng. **5**, 603 (1987).
[4] L. C. Chhabildas, J. L. Wise, and J. R. Asay, in *Shock Waves in Condensed Matter-1981*, edited by W. Nellis, L. Seaman, and R. Graham (American Institute of Physics, New York, 1982), p. 422.
[5] J. R. Asay, L. C. Chhabildas, and D. P. Dandekar, J. Appl. Phys. **51**, 4774 (1980).
[6] J. R. Asay and L. C. Chhabildas, in *Shock Waves and High-Strain Rate Phenomena in Metals*, edited by M. Meyers and L. Murr (Plenum, New York, 1981), p. 417.
[7] K. G. Hoge and A. K. Mukherjee, J. Mater. Sci. **12**, 1666 (1977).
[8] M. L. Wilkins, Calculations of Elastic-Plastic Flow, Lawrence Livermore National Laboratory, Rep. No. UCRL-7322, Rev. 1 (1969).
[9] J. E. Dorn and S. Rajnak, Trans. Metall. Soc. AIME **230**, 1052 (1964).
[10] P. Guyot and J. E. Dorn, Can. J. Phys. **45**, 983 (1967).
[11] D. Klahn, A. K. Mukherjee, and J. E. Dorn, in *Proceedings of the 2nd International Conference on the Strength of Metals and Alloys*, Pacific Grove, CA, 1970 (American Society for Metals, Cleveland, 1970), Vol. 3, p. 951.
[12] W. M. Isbell, D. R. Christman, and S. G. Babcock, Measurements of Dynamic Properties of Materials VI: Tantalum, Materials and Structures Laboratory, General Motors Technical Center, Warren, Michigan, DASA 2501-6, MSL-70-23, Vol. VI, pp. 8 and 33 (1972).
[13] R. G. McQueen, S. P. Marsh, J. W. Taylor, J. N. Fritz, and W. J. Carter, in *High-Velocity Impact Phenomena*, edited by R. Kinslow (Academic, New York, 1970), p. 293.
[14] D. Banner, Lawrence Livermore National Laboratory, 1974 (unpublished).
[15] C. E. Morris, Ed., *Los Alamos Shock Wave Profile Data* (University of California, Berkeley, 1982), p. 41.
[16] D. Grady, Sandia National Laboratory, 1983 (unpublished).